# Activation of Intact Bacteria and Bacterial Fragments Mixed with Agar as Cloud Droplets and Ice Crystals in Cloud Chamber Experiments

Kaitlyn J. Suski,[1] David M. Bell,[1] Naruki Hiranuma,[2,3] Ottmar Möhler,[2] Dan Imre,[4] and Alla Zelenyuk[1]

5   [1]Pacific Northwest National Laboratory, Richland, WA, USA.
[2]Institute of Meteorology and Climate Research – Atmospheric Aerosol Research, Karlsruhe Institute of Technology, Karlsruhe, Germany.
[3]Currently at Department of Life, Earth and Environmental Sciences, West Texas A&M University, Canyon, TX, USA.
[4]Imre Consulting, Richland, WA, USA

10   *Correspondence to:* Alla Zelenyuk (alla.zelenyuk-imre@pnnl.gov)

**Abstract.** Biological particles, including bacteria and bacterial fragments, have been of much interest due to the special ability of some to nucleate ice at modestly low temperatures. This paper presents results from a recent study conducted on two strains of cultivated bacteria which suggest that bacterial fragments mixed with agar, and not whole bacterial cells, serve as cloud condensation nuclei (CCN). Due to the absence of whole bacteria cells in droplets, they are unable to serve as ice nucleating

15   particles (INPs) in the immersion mode under the experimental conditions. Experiments were conducted at the Aerosol Interaction and Dynamics in the Atmosphere (AIDA) cloud chamber at the Karlsruhe Institute of Technology (KIT) by injecting bacteria-containing aerosol samples into the cloud chamber and inducing cloud formation by expansion over a temperature range of -5 to -12 °C. Cloud droplets and ice crystals were sampled through a pumped counterflow virtual impactor inlet (PCVI) and their residuals were characterized with a single particle mass spectrometer (miniSPLAT). The size distribution

20   of the overall aerosol was bimodal, with a large particle mode composed of intact bacteria and a mode of smaller particles composed of agar mixed with bacterial fragments that were present in higher concentrations. Results from three expansions with two bacterial strains indicate that the cloud droplet residuals had virtually the same size distribution as the smaller particle size mode and had mass spectra that closely matched those of agar and bacterial fragments. The characterization of ice residuals that were sampled through an ice-selecting PCVI (IS-PCVI) also shows that the same particles that activate to form cloud

25   droplets, bacteria fragments mixed with agar, were the only particle type observed in ice residuals.

## 1 Introduction

Aerosols affect climate directly, by scattering and absorbing solar and terrestrial radiation and indirectly through interactions with clouds and precipitation (IPCC, 2013). In their role as cloud condensation nuclei (CCN) and ice nucleating particles (INPs), aerosol particles affect cloud microphysical properties (Pruppacher and Klett, 2010). Biological particles, including

30   bacteria, which are found in the atmosphere in various forms but at relatively low number concentrations, might play an

important role globally as CCN or INPs. While a large body of work on the ice nucleating (IN) activity of biological particles exists, the extent of their role in ice formation within modestly supercooled clouds remains poorly understood ((Murray et al., 2012) and references therein).

Previous studies that looked at the CCN activity of bacteria concluded that bacteria range from very hygroscopic, and hence CCN active under atmospherically relevant conditions (Bauer et al., 2003), to only slightly hygroscopic, activating only at critical supersaturations close to or exceeding those indicating wettability (Franc and DeMott, 1998). It has been suggested, based on contact angle measurements (Sharma and Rao, 2002), that these differences reflect a range of bacteria cell wall types, some of which are hydrophilic, while others are hydrophobic. However, most of these studies utilized aerosolized suspensions of cultured cells that include, in addition to intact bacteria with well-defined cell walls, bacterial fragments mixed with agar growth medium in which the bacteria were cultured (Wolf et al., 2015). Particles composed of bacterial fragments mixed with hygroscopic agar are expected to activate into cloud droplets more efficiently than their whole cell counterparts, which are enclosed in a hydrophobic shell. Although it's been suggested that biological particles may serve as giant CCN (Möhler et al., 2007), in most cases, atmospheric air parcels contain many types of CCN active particles and few biological particles, diminishing the importance of bacteria for liquid cloud activation. In contrast, the fact that bacterial samples have been shown to induce ice formation at relatively warm temperatures suggests that they might play an important role as INPs in mixed phase clouds (Möhler et al., 2007).

Depending on the INP composition and size, and on the temperature and relative humidity (RH), ice formation can occur by several pathways. The freezing modes most relevant to bacteria particles are *immersion freezing*, which is induced by a particle immersed in supercooled water ((Murray et al., 2012;Vali et al., 2015) and references therein); *condensation freezing*, in which water condensing on an INP freezes; and *contact freezing* that occurs when a liquid droplet hits an INP and freezes on contact. However, for the experiments presented here immersion freezing represents the primary ice formation mechanism. In immersion freezing, the INP first activates as a liquid cloud droplet, when the RH over water ($RH_w$) exceeds 100% RH, and ice forms when this droplet freezes due to the presence of a solid nucleus, which means that this ice formation mechanism is tightly connected to the particle CCN activity.

Many biological particle types including pollen (Hader et al., 2014;Augustin et al., 2013), fungi (Fröhlich-Nowoisky et al., 2015), and decaying plant material (Schnell and Vali, 1976;Conen et al., 2016) have been identified as efficient INPs. Additionally, nano-INPs have been observed from fungi (O'Sullivan et al., 2016), pollen (Pummer et al., 2012), and proteins from IN active bacteria (Wolber et al., 1986). These IN active proteins were shown to be active on their own, in the absence of intact bacteria, demonstrating that a single protein is all that is required to initiate freezing (Govindarajan and Lindow, 1988). Additionally, IN active bacterial fragments have been observed in the ambient environment (Šantl-Temkiv et al., 2015).

A previous study at the AIDA cloud chamber concluded that both bacterial fragments and whole cells were CCN and IN active, with whole cells being slightly more IN active than the fragments, and the fragments having a higher hygroscopicity than the

whole cells (Oehm, 2012). Several other studies have reached similar conclusions indicating that both whole cells and bacterial fragments serve as INPs (Wex et al., 2015;Hartmann et al., 2013;Yankofsky et al., 1981). In contrast, an earlier study at the AIDA chamber suggested that only intact bacteria are IN active (Möhler et al., 2008). The distinction between whole cells and bacterial fragments is important from many perspectives, especially when calculating available surface area, surface site density, and active or frozen fraction of bacteria in laboratory experiments. More importantly, modeling studies suggest biological particles may be an important player in precipitation processes (Burrows et al., 2013;Morris et al., 2004), but because atmospheric concentrations of intact bacteria and bacterial fragments are poorly constrained and expected to be vastly different, it remains uncertain how big of a role bacteria play in mixed phase cloud formation globally.

When interpreting previously published studies, it is important to keep in mind that when a solution containing cultivated bacterial cells is aerosolized, at least two types of particles form: Intact or whole bacterial cells and small particles, composed of bacterial fragments mixed with agar. The size distribution of the small particle mode depends on the particles generation, i.e. the size of aerosolized droplets, and the concentration of the agar and bacterial fragments in the solution/suspension. Therefore, it would not be surprising to find that its number concentration and size distribution differ from one experimental set-up to the next, and that it could even change with the age of the solution/suspension.

The data presented here were acquired during cloud simulation experiments performed at the AIDA cloud chamber during the first part of the Fifth International Ice Nucleation Workshop (FIN-1). The single particle mass spectrometer, miniSPLAT (Zelenyuk et al., 2015), was utilized to characterize the size and chemical compositions of intact bacteria cells and bacterial fragments mixed with agar before and after cloud formation. Most importantly, it was used to characterize the residuals of liquid droplets and ice crystals formed during the expansions. Cloud particles were separated from interstitial particles with a pumped counterflow virtual impactor (PCVI) or an ice-selecting PCVI (IS-PCVI) (Hiranuma et al., 2016). Comparison between the properties of cloud residuals with the overall particle population in the chamber before and after the expansion allows for the determination of cloud and ice active versus interstitial particles.

As it will be demonstrated below, the results of these measurements, on two different bacteria, indicate that bacterial fragments mixed with agar accounted for the clear majority of particles active as CCN and as INPs, while whole cells activated with much lower probability, if at all.

## 2 Experimental

The Fifth International Ice Nucleation Workshop (FIN) was a three-part study that aimed to compare a number of single particle mass spectrometers and ice nucleation instruments. The data presented here were collected during FIN-1, which took place in November of 2014 at the AIDA cloud chamber at KIT in Karlsruhe, Germany. Ten single particle mass spectrometers from several research groups around the world were brought together for FIN-1 to simultaneously characterize the size and

composition of various types of aerosol particles, including those being used in the AIDA chamber to study their activity as CCN and INPs.

The AIDA cloud chamber and its operation were previously described in detail elsewhere (Möhler et al., 2003). Briefly, the AIDA cloud chamber is an 84 m$^3$ aluminum vessel in a thermally insulated housing that can be set to a desired relative humidity

5  (RH), temperature, and pressure. To induce cloud formation, the pressure of the chamber, filled with aerosol particles, is lowered by pumping on the chamber, which causes the gas to expand, the temperature to drop, and the relative humidity (RH) to increase above ice saturation, depending on the specific experiment. Once supersaturation with respect to water is reached at temperatures below 0°C, cloud droplets, and eventually ice crystals, form. The data presented in this paper are from 3 expansions during the campaign, Expansions 36, 37, and 38, which are referred to as Expansions 1, 2, and 3, respectively,

10  throughout this paper. The mobility size distributions of particles in the AIDA chamber are measured before and after expansions with a scanning mobility particle sizer (SMPS), comprised of a differential mobility analyzer (DMA, TSI Inc., Model 3080) and a condensation particle counter (CPC, TSI Inc., Model 3010). The SMPS sizes particles with mobility diameters larger than 14 nm and smaller than 740 nm, while larger particles, with aerodynamic diameters from 0.5 to 20 µm, are sized with an aerodynamic particle sizer (APS, TSI Inc., Model 3321). Throughout the manuscript the combined SMPS

15  and APS data are shown as volume-equivalent diameters calculated using a particle density of 1.4 g/cm$^3$ and a dynamic shape factor of 1. Total particle number concentrations are measured with a CPC (TSI Inc., Model 3076). Temperature and RH are measured using a number of calibrated sensors (Fahey et al., 2014;Möhler et al., 2003). Optical diameters of cloud droplets and ice crystals are determined using two optical particle counters (welas OPCs, Palas GmbH, sensor series 2300 and 2500). The detection size ranges of the two OPCs, referred to as welas1 and welas2, are ~0.7 to 46 µm and ~5 to 240 µm, respectively

20  (Wagner and Möhler, 2013). The simultaneous use of these two OPCs effectively spans the size range of droplets and ice crystals formed in the chamber.

A pumped counterflow virtual impactor (PCVI) (Boulter et al., 2006) and an ice-selecting PCVI (IS-PCVI) (Hiranuma et al., 2016) were used to selectively sample cloud droplet and ice crystals, the residuals of which were counted with the CPC and characterized by miniSPLAT and other instruments. PCVIs use a counterflow to reject smaller, interstitial particles, while

25  particles that have enough inertia to pass through the counterflow are transmitted through the inlet. The ratio of the counterflow to the pumped flow changes the inlet cut-size. One advantage of using the PCVI system is to provide residual-laden flows, in which particles are virtually concentrated by a flow concentration factor (i.e., the ratio of input flow to output flow), to the downstream instruments. The IS-PCVI, which has a higher cut-size than other PCVIs (Hiranuma et al., 2016), is intended to be used to reject both interstitial particles and small cloud droplets and allow the larger ice crystals through. The heated

30  evaporation sections installed downstream of each PCVI are maintained at a temperature above 35 °C to evaporate water from the cloud particles leaving the residuals behind.

Vacuum aerodynamic diameters ($d_{va}$) and chemical compositions of individual aerosol particles and cloud residuals were measured with miniSPLAT, a single particle mass spectrometer, a detailed description of which is given elsewhere (Zelenyuk

et al., 2015). Briefly, individual aerosol particles enter miniSPLAT through an aerodynamic lens inlet (Vaden et al., 2011a) and are detected by light scattering in two optical stages 10.9 cm apart. The time it takes the particles to pass between the two continuous laser beams (532 nm Nd:YAG CrystaLaser, Model CL-300-LO) yields particle velocity, which for a given inlet pressure is related to particle $d_{va}$. Given that the inlet pressure is changing during expansions, a pressure-dependent size calibration was developed and used. The dual particle detection is also used to generate a trigger for the excimer laser (GAM Lasers Inc., Model EX-5), operated at 193 nm, which ablates the particles and generates positive and negative ions. Single particle mass spectra are obtained with a dual-polarity, z-configuration reflectron time-of-flight mass spectrometer (Z-TOF, Tofwerk AG). All data generated by miniSPLAT are processed, analyzed, and visualized using custom software (Zelenyuk et al., 2008;Zelenyuk et al., 2006).

Suspensions of cultured Pseudomonas syringae and PF CGina 01 were prepared, as described in Hiranuma et al. (2016), by suspending ~$10^9$ bacteria cells mL$^{-1}$ in sterile water and a small amount of Kings Base Agar. The solutions were atomized using a custom atomizer (Wex et al., 2015), dried by flowing through two diffusion driers (TOPAS, Model DDU 570), and injected into the AIDA chamber prior to expansions.

## 3 Results and Discussion

Prior to each experiment, the AIDA cloud chamber was preconditioned overnight to reach the desired experimental temperature. Before the 1$^{st}$ expansion presented here (Expansion 1), a suspension of Pseudomonas syringae bacteria was aerosolized, dried, and the resulting particles were introduced into the chamber. Figure 1 shows the calculated volume equivalent diameter ($d_{ve}$)size distributions of particles present in AIDA before the expansion, which was obtained by combining measurements by the SMPS (black line) and the APS (red line). Figure 1a shows a smaller size mode that peaks at ~70 nm and a broad peak at ~800 nm. The miniSPLAT-measured vacuum aerodynamic size ($d_{va}$) distribution, shown in Figure 1b, also has two distinct peaks at 180 nm and ~850 nm, for the small and large size modes, respectively. The difference between the small particle peak positions of the measured $d_{va}$ and $d_{ve}$ size distributions is due to particle density ($\rho > 1$ g cm$^{-3}$) and the miniSPLAT's small particle detection limit (50% cut off at 85 nm, marked with a green line in Figure 1a) (Vaden et al., 2011b). This type of bimodal size distribution has been observed previously with other aerosolized suspensions of cultivated bacteria (Wex et al., 2015;Wolf et al., 2015;Möhler et al., 2008). The large size mode corresponds to intact/whole bacteria cells and the smaller mode is composed of bacterial fragments mixed with agar.

Representative positive and negative ion mass spectra (MS) of the two particle modes are shown in Figure 2. The reference MS of the small particle mode includes MS of particles smaller than 300 nm and that of the large particle mode/intact bacteria includes the MS of particles larger than 700 nm. Comparison between the reference MS of the two particle modes shows that nearly all the peaks are present in the MS of both modes. However, the positive ion MS of the two modes exhibit significantly different relative peak intensities, while the negative ion MS are very similar. The positive ion MS indicate the presence of

many organics and metal ions, including sodium ($^{23}Na^+$), potassium ($^{39/41}K^+$), calcium ($^{40}Ca^+$) and calcium oxides ($^{56}CaO^+$, $^{113}(CaO)_2H^+$). The negative ion MS show the presence of organic nitrogen ($^{26}CN^-$, $^{42}CNO^-$), chloride ($^{35/37}Cl^-$), and phosphates ($^{63}PO_2^-$, $^{79}PO_3^-$). The positive ion MS for intact cells show relatively lower intensities for the metal ions ($^{23}Na^+$, $^{39/41}K^+$, $^{40}Ca^+$) and significantly higher intensities for the organic peaks as compared to those of the small particle mode, which are dominated

5    by the potassium peak. The same MS are presented in Figure S1 in expanded scale together with the MS of pure agar particles. Comparison between MS of agar and the small particle mode shows their positive ion MS to be nearly identical, while the negative ion MS are significantly different, with the agar MS containing no phosphate peaks. The size distributions and MS provide direct evidence that the smaller particles are composed of agar *mixed* with bacterial fragments, while the larger size particle mode corresponds to intact bacteria cells. The MS of intact bacteria shown in Figures 2 and S1 are similar to previously

10   published single particle mass spectra of laboratory-generated Pseudomonas syringae acquired by two other single particle mass spectrometers (Pratt et al., 2009;Zawadowicz et al., 2017). The negative ion MS are virtually the same, while the positive ion MS presented here exhibit significantly higher intensity in organic peaks, most likely due to the differences in the ablation laser wavelength or power. Moreover, these studies do not mention the presence of two particle size modes.

The size distributions shown in Figure 1a indicate a total number concentration of particles in the chamber of ~2,500 particles

15   cm$^{-3}$, ~1,000 particles cm$^{-3}$ of which are larger than 100 nm, and only ~100 particles cm$^{-3}$, or 4%, are intact bacteria. In comparison, the $d_{va}$ size distribution (Figure 1b) yields 7% for the fraction of intact bacteria, since more than half of the particles in the smaller size mode are too small to be detected by miniSPLAT. It is important to point out that the size, number concentration, and the relative fraction of the small particles containing bacterial fragments can vary from experiment to experiment and that they are determined by the solution/suspension concentrations of agar, intact bacteria, and cell fragments,

20   as well as how the bacteria culture is grown and prepared for the experiment (Wolf et al., 2015), and could even change with the age of the solution/suspension. Given the differences in dry size, composition, and hygroscopicity of these two particle types, they might be expected to have different cloud droplet and ice nucleation activities.

Cloud formation is induced by lowering the pressure in the AIDA chamber, using active pumping, which lowers the pressure and temperature of the gas in the chamber and increases the RH, which is shown in Figure 3a. As the chamber became

25   supersaturated with respect to both ice and water, cloud droplets and ice crystals formed, which is illustrated in Figure 3b with a false color plot of the welas2-measured size distribution as a function of expansion time. As the temperature decreased and the RH increased, the number concentrations of droplets larger than 5 µm rapidly increased. After ~500 sec, as pumping stopped, the temperature increased, RH dropped, and the droplet number concentration decreased mainly due to evaporation. During the expansion, the vast majority of the droplets remained smaller than 14 µm. The few ice crystals that formed are

30   apparent in the figure as a second mode of much larger particles (marked in Figure 3b) mainly visible at ~100 to 200 sec, after which point their numbers rapidly decreased mainly because of settling losses.

The welas2 data are also plotted in Figure 3c in a 2D plot format. The figure shows that the number concentration of cloud droplets and ice crystals (particles larger than 5 µm, plotted as a black line) quickly reaches ~900 particle cm$^{-3}$ and then

decreases slowly to 400 particles cm$^{-3}$, before it rapidly drops to zero. Ice crystal concentrations derived from welas2-measured number concentrations of particles larger than 30 μm are indicated by the pink line in Figure 3c. Ice crystals appear later in the expansion, and their numbers reach a maximum of 3 particles cm$^{-3}$, or more than 200 times lower than droplets. As a reminder, before the expansion, there were ~ 2,500 particles cm$^{-3}$ in the chamber, including only ~100 intact bacteria cm$^{-3}$.

5    Early in the expansion when there were mostly droplets present in the chamber, the number of cloud particles reached 900 particles cm$^{-3}$, signifying a very high CCN activation efficiency of particles composed of bacterial fragments mixed with agar.

The CPC and miniSPLAT-measured number concentrations of cloud residuals transmitted through the PCVI, shown in Figure 3c in yellow and green, respectively, exhibit very similar behavior. These data indicate a rapid increase early in the expansion and a relatively fast drop to zero after ~250 sec, with the temporal evolution of the two independently measured residuals number concentrations showing good agreement. Figures 3b and 3c show that during Expansion 1 the PCVI transmitted predominantly droplets, the residuals of which were characterized by the CPC and miniSPLAT.

The $d_{va}$ size distribution of cloud residuals measured by miniSPLAT is presented together with the $d_{va}$ size distribution of the particles in the chamber before the expansion in Figure 4. The miniSPLAT-measured size distribution of particles composed of agar and bacterial fragments before the expansion and of cloud residuals are virtually the same, and the intact bacteria, i.e. the large particle mode, is "missing" from the size distribution of the cloud residuals. These data provide direct evidence that under the experimental conditions in Expansion 1, particles composed of bacterial fragments mixed with agar preferentially activated to form cloud droplets, a small fraction of which became ice crystals, as illustrated in Figure 3.

In addition to the $d_{va}$ size distribution, miniSPLAT measured positive and negative ion MS of individual cloud residuals, which are presented in Figure 5 superimposed on the reference MS of intact bacteria (large mode particles) (Figure 5a and b) and on the reference MS of the small particle mode composed of agar and bacterial fragments (Figure 5c and d) measured before the expansion. Comparison between the three particle types shows that the cloud residuals have nearly the same MS as that plotted in Figure 2a for the small particle mode in the chamber before the expansion. This suggests that the bacteria fragments mixed with agar are serving as CCN, which is consistent with the conclusions based on the measured $d_{va}$ size distributions. The small differences between the MS of residuals and the small particle mode suggest a slightly higher content of organics in the residuals, which is due to the fact that the MS of residuals includes all detected particles, while the reference MS of the small particle mode includes only particles smaller than 300 nm. These MS differences will be further examined below in a detailed analysis of data obtained during Expansion 2, where the observed differences are larger and, therefore, easier to analyze.

In summary, prior to Expansion 1 there were ~2,500 particles cm$^{-3}$ in the chamber, ~10% of which were intact bacteria. During the expansion, the maximum number of droplets formed reached 900 particles cm$^{-3}$, and the average droplet concentration was 650 particles cm$^{-3}$, while the maximum ice crystal concentration was 3 particles cm$^{-3}$ and the average was slightly less than 1 crystal cm$^{-3}$. As a result, the clear majority of the particles transmitted through the PCVI were droplets. The miniSPLAT-measured $d_{va}$ size distribution of the cloud residuals is nearly identical to that of the small particle mode. Consistent with the

size distribution, the MS of the cloud residuals is nearly the same as the reference MS of the small particle mode, demonstrating preferential droplet activation of smaller particles composed of bacterial fragments mixed with agar, as well as, the absence of intact cells in droplets residuals.

Expansion 2 was performed in the same exact manner as Expansion 1, except that a different bacteria, cultivated PF CGina01,

5  was used. Figure 6a presents the size distributions of particles in the chamber prior to Expansion 2, showing two particle modes, the small size mode, composed of agar and bacterial fragments, which peaks at 60 nm, and the intact bacteria, which peaks at $d_{ve} \approx 700$ nm. There were 1,800 particles cm$^{-3}$, ~4% of which were intact bacteria. Similarly, the $d_{va}$ size distribution, shown in Figure 6b, indicates two particle modes: the small size mode peaking at $d_{va} \approx 160$ nm, composed of agar and bacterial fragments , and the intact bacteria mode, which peaks at $d_{va} \approx 850$ nm and represents ~9% of particles detected and sized by

10  miniSPLAT prior to Expansion 2. Comparison between the reference MS of the two particle modes present before Expansion 2 is presented in Figure 7, where the small mode includes particles smaller than 300 nm, and the large mode represents particles larger than 700 nm. As in the case of Expansion 1, the MS show that the small particles are composed of agar and bacterial fragments, as evident by the presence of phosphate peaks in the negative ion MS. The difference between the two positive ion reference MS for PF CGina01 is very similar to the pattern observed for Pseudomonas syringae bacteria (Figure 2).

15  The temporal evolution of pressure, temperature, and RH during Expansion 2 are shown in Figure 8a. The welas2-measured size distributions of cloud particles as a function of time, shown in Figure 8b as a false color image, reveal that most of the activated particles were liquid droplets smaller than 10 μm, and that only a small number of cloud particles were ice crystals, as determined by their significantly larger optical diameters. The analysis of the welas2-measured number concentrations of cloud droplets and ice crystals as a function of time presented in Figure 8c indicates that the average droplet and ice crystal

20  concentrations were ~730 particles cm$^{-3}$ and ~1 particle cm$^{-3}$, respectively, with ice crystal peak concentrations reaching ~3 particles cm$^{-3}$ at 150 to 250 seconds from the start of the expansion. As a result, particles transmitted through the PCVI to the CPC and miniSPLAT during Expansion 2 were predominantly liquid droplets. The CPC- and miniSPLAT-measured number concentrations of particles transmitted by the PCVI, also presented in Figure 8c, show rapid increases early in the expansion and slower decreases thereafter, displaying the same behavior as in Expansion 1.

25  The miniSPLAT-measured $d_{va}$ distributions of cloud residuals (blue) and particles in the chamber prior to the expansion (green) are shown in Figure 9. As with Expansion 1, the $d_{va}$ distribution of cloud residuals is nearly identical to that of the small particle mode present in the chamber before the expansion. An expanded scale of the intact bacteria size region, shown in the figure inset, indicates no detectable intact bacteria in cloud residuals.

The average positive ion MS of cloud residuals is shown in Figure 10. For comparison, it is superimposed on the reference

30  MS of the small particle mode (Figure 10a) and intact bacteria (Figure 10b). The MS of residuals shows that they contain slightly more organics than the particles that were included in the reference MS of the small particle mode. It is important, however, to note that the residual MS includes all particles, while the reference MS contains only particles smaller than 300

nm. A possible explanation for the observed difference between the two MS is that the organic content of the small particle mode increases with particle size, i.e. larger particles contain more or larger bacterial fragments and, hence, relatively less agar. Indeed, Figure 11 shows that the fraction of organics (peaks at $m/z \geq 44$) relative to $K^+$, which serves as a simple qualitative measure of the relative fraction of bacterial fragments and agar in these particles, is increasing with particle size.

5 As a reminder, a schematic representation of the measured $d_{va}$ size distribution of cloud residuals, is shown in dashed blue line. For comparison, the same analysis applied to the MS of pure agar and intact bacteria particles yields 86% and 13% for the $K^+$ MS peak, respectively. The MS of cloud residuals smaller than 300 nm, shown in Figure S2a, are nearly identical to the reference MS of the small particle mode, i.e. bacterial fragment mixed with agar particles smaller than 300 nm, while the MS of cloud residuals that are larger than 300 nm, which in this expansion were dominated by particles whose $d_{va}$ is ~500 nm, is

10 similar, but not exactly the same, as the reference MS of intact bacteria, as shown in Figure S2b. These small differences are not sufficient to eliminate the possibility that some of the cloud activated larger particles are in fact small intact bacteria.

Overall, the $d_{va}$ size distributions and MS of cloud residuals are like those of the small particle mode, although the larger residuals, which contain more organics, could be smaller intact bacteria. The data clearly show that the vast majority of intact bacteria in the chamber did not activate. In all respects, the miniSPLAT data for PF CGina01 are consistent with those for

15 Pseudomonas syringae (Expansion 1) and confirm the preferential droplet activation of particles composed of agar mixed with bacterial fragments.

Expansion 3 followed the same pumping strategy and expansion temperatures as the previous expansions, but was conducted on particles which remained in the AIDA chamber after Expansion 2. The $d_{ve}$ size distributions of these particles, shown in Figure 6a as dashed lines, are nearly identical to those measured before Expansion 2, despite a decrease in the total particle

20 number concentration. During Expansion 3, the cloud residual particles, sampled by the CPC and miniSPLAT, were transmitted through the IS-PCVI in order to reduce the number of droplets transmitted to allow for characterization of ice crystal residuals.

Changes in chamber pressure, temperature, and RH for Expansion 3 are shown in Figure 12a. A false color plot of the activated particles size distribution measured by welas2, as a function of time, is presented in Figure 12b. Figure 12c displays the welas2-

25 measured total number of activated particles as a function of time (black), which almost reaches 700 particles cm$^{-3}$, indicating a very high CCN activation efficiency. In addition, it shows the number concentrations of cloud particles with optical diameters larger than 15 µm but smaller than 20 µm (light blue) and the number of particles larger than 20 µm (pink). The former may correspond to the number of droplets transmitted by the IS-PCVI, while the latter may be relevant to transmitted ice crystals. Comparison between the two shows that the IS-PCVI transmitted nearly equal numbers of ice crystals and droplets to

30 miniSPLAT and the CPC. miniSPLAT and the CPC-measured particle number concentrations are also shown in Figure 12c. Both instruments show a rapid rise in the concentration of cloud residuals, followed by a significant drop in concentration with time. Early in the expansion, most of the transmitted particles are droplets, but later the number of droplets and ice crystal residuals becomes comparable, as shown in Figure 12c.

Two particle modes are present in the $d_{va}$ size distribution of particles in the chamber before Expansion 3 (Figure 13, green trace). Figure 13 also shows the $d_{va}$ size distributions of all cloud residuals detected throughout the expansion (blue) and cloud residuals detected late in the expansion, when the number concentration of droplets and ice crystals were approximately equal (light blue). Both cloud residual size distributions are nearly the same as that of the small particle mode and show no distinct

5   peak in the size region of intact bacteria.

The average MS of particles sampled through the IS-PCVI throughout the expansion and later in the expansion are shown in Figure 14. The fact that the two MS are virtually identical suggests that the compositions of particles that remain as droplets and those that activate into ice crystals are not different, which is consistent with the finding that the size distributions are the same.

10  The residual size distributions and compositions combined again confirm that the majority of particles that served as CCN and INPs were bacterial fragments mixed with agar. While there is no clear indication that intact bacterial cells were activated, it cannot be ruled out that larger cloud residuals were small intact bacteria mixed with agar.

These results are consistent with previous studies that show that whole cells are not necessary for ice formation because IN active proteins and protein complexes can serve as INPs (Lindow et al., 1989;Maki and Willoughby, 1978;Hartmann et al.,

15  2013;Govindarajan and Lindow, 1988). However, it has generally been assumed that whole cells will also nucleate ice (Möhler et al., 2008;Wex et al., 2015;Lindow et al., 1989) and are more active than a single IN active protein (Govindarajan and Lindow, 1988) or bacterial fragment (Yankofsky et al., 1981;Hartmann et al., 2013). The suggestion is that IN active proteins collect in the cell membrane (Lindow et al., 1989;Govindarajan and Lindow, 1988) and become concentrated on the surface of intact cells enhancing the IN activity of intact bacteria. Nevertheless, the data presented here show that bacterial fragments

20  mixed with agar preferentially activate as droplets and are the only particles observed in ice residuals.

## 4 Conclusions

This paper presents the results of measurements of particle number concentrations, size distributions, and compositions of aerosol particles produced from two types of bacteria particles in the AIDA chamber for three expansions, before and after the expansions. In all cases, the data show the presence of two distinct particle types in the chamber: particles larger than ~ 700

25  nm that are intact bacteria, and small particles, with a $d_{ve}$ distribution that peaks at ~65 nm, that are composed of agar mixed with bacterial fragments. The MS show that the small and large particles have distinct MS, representing differences in particle compositions. The small particles are composed of a mixture of bacterial fragments and agar, as determined by comparison with the MS of pure agar particles and intact bacteria. In addition, a detailed analysis of the MS of all particles shows that the organic content of particles relative to potassium increases with particle size, indicating that smaller particles are dominated

30  by agar, whereas larger particles have more organics, i.e. bacterial fragments and/or bacterial cells.

The concentration of small particles in the chamber was about thirty times higher than that of intact bacteria for all expansions. The two particle modes in the chamber were detected before and after the three expansions, providing direct evidence that intact bacteria remain intact throughout the expansion.

In the three expansions presented here, cloud activation occurred between –5 and -12 °C to form cloud droplets, a small fraction of which froze into ice crystals. The cloud droplets had a wide size distribution of optical diameters that peaked at about 8 µm with some being as large as 15 µm. Ice crystals had a very wide size distribution with some having optical diameters as large as 200 µm. Cloud droplet concentrations were ~30% of the total particle number concentration in the AIDA chamber, which is significantly higher than the concentration of intact bacteria.

The cloud particles were separated with the PCVI or IS-PCVI, and their residuals were characterized with miniSPLAT. The data in all three expansions present virtually the same picture. The $d_{va}$ size distributions of cloud residuals were devoid of the large particle/ intact bacteria mode and were nearly the same as the miniSPLAT-measured $d_{va}$ distributions of the small particle/ bacterial fragment mode acquired before and after the expansions, providing direct evidence that most of the particles that activated to form either droplets or ice crystals were bacterial fragments mixed with agar. The similarity between the $d_{va}$ distributions of the small particle mode and the cloud residuals is consistent with the relatively high droplet activation probability and the fact that on the small particle side the $d_{va}$ distribution is determined by the instrument detection limit.

MS analysis of the cloud residuals confirms that, while both intact bacterial cells and bacterial fragments mixed with agar were present in the AIDA chamber before and after the expansions, the latter represented a clear majority of particles that served as CCN and as INPs. These results were replicated for two different bacteria strains, Pseudomonas syringae and PF CGina 01, suggesting that this behavior may be representative of bacteria in general, or at least of cultivated bacteria used in most laboratory experiments.

It is important to note that at the activation temperatures and RHs of the three expansions presented here, particles first activate as CCN to form cloud droplets and ice crystals form by immersion freezing. If the reports suggesting that intact bacteria are not hygroscopic are correct, it is not surprising to find that intact bacteria have limited CCN activity, and by necessity, a negligible amount can serve as INP in the immersion mode. Drop freezing and other bulk immersion freezing techniques bypass the issue of limited hygroscopicity by submerging whole cells in a droplet or well of water, artificially overcoming the barrier of CCN activation. These distinctions are important to consider when relating laboratory INP measurements to estimations of ice formation in clouds. A recent modeling study has shown that competition for water vapor can inhibit ice formation in clouds due to the most CCN-active particles taking up all the water and leaving the more IN active, but less CCN active, particles as interstitial aerosol and thus, unable to form ice in clouds (Simpson et al., 2017). The study presented here shows that, in contrast to intact bacteria, particles composed of bacterial fragments mixed with agar are CCN active and a fraction of their resulting cloud droplets freeze to make ice crystals. While agar is hygroscopic, pure agar particles do not

freeze to form ice crystals at the temperature range examined in this study, indicating that the bacterial fragments served as INPs in these expansions.

If agar is essential to transforming bacterial fragments into effective CCN and INP, as the data presented here suggest, then in the ambient atmosphere bacterial fragments might not be IN active unless mixed with hygroscopic substances that can enhance the CCN activity. Thus, it is important to quantify the role agar plays in CCN and IN activity of bacteria by conducting experiments on bacterial samples that contain no agar. Similarly, it is important to investigate the effect of atmospherically relevant hygroscopic compounds, like sulfates and nitrates, which could coat bacterial fragments suspended in the atmosphere transforming them into CCN and IN active particles.

*Data availability.* The data used in this manuscript are available at https://dtn2.pnl.gov/data/release/2018_Suski_et_al_Bacteria_Paper/.

*Competing interests.* The authors have no conflict of interest.

*Special issue statement.* This article is part of the special issue "Fifth International Workshop on Ice Nucleation (FIN)". It is not associated with a conference.

*Acknowledgments.* Support for AZ, DMB, and KS was provided by the U.S. Department of Energy (DOE) Office of Biological and Environmental Research (OBER) Atmospheric Research Systems Program (ASR). Development of miniSPLAT was funded by the DOE Office of Science, Office of Basic Energy Sciences, Division of Chemical Sciences, Geosciences & Biosciences and EMSL User Facility sponsored by the DOE OBER and located at Pacific Northwest National Laboratory. The valuable contributions of the FIN organizers, their institutions, and the FIN-1 Workshop science team are also gratefully acknowledged. OM and NH thank the Engineering and Infrastructure group members at KIT IMK-AAF (Georg Scheurig, Tomasz Chudy, Rainer Buschbacher, Olga Dombrowski, Steffen Vogt, Jens Nadolny and Frank Schwarz) for their technical support during FIN-1. The AIDA work was partly funded by the Helmholtz Association through its research programme 'Atmosphere and Climate (ATMO)'.

## References

Augustin, S., Wex, H., Niedermeier, D., Pummer, B., Grothe, H., Hartmann, S., Tomsche, L., Clauss, T., Voigtländer, J., Ignatius, K., and Stratmann, F.: Immersion freezing of birch pollen washing water, Atmos. Chem. Phys., 13, 10989-11003, 10.5194/acp-13-10989-2013, 2013.

Bauer, H., Giebl, H., Hitzenberger, R., Kasper-Giebl, A., Reischl, G., Zibuschka, F., and Puxbaum, H.: Airborne bacteria as cloud condensation nuclei, J Geophys Res-Atmos, 108, 10.1029/2003jd003545, 2003.

Boulter, J. E., Cziczo, D. J., Middlebrook, A. M., Thomson, D. S., and Murphy, D. M.: Design and performance of a pumped counterflow virtual impactor, Aerosol Sci Tech, 40, 969-976, Doi 10.1080/02786820600840984, 2006.

5    Burrows, S. M., Hoose, C., Poschl, U., and Lawrence, M. G.: Ice nuclei in marine air: biogenic particles or dust?, Atmos Chem Phys, 13, 245-267, DOI 10.5194/acp-13-245-2013, 2013.

Conen, F., Stopelli, E., and Zimmermann, L.: Clues that decaying leaves enrich Arctic air with ice nucleating particles, Atmospheric Environment, 129, 91-94, http://dx.doi.org/10.1016/j.atmosenv.2016.01.027, 2016.

Fahey, D. W., Gao, R. S., Möhler, O., Saathoff, H., Schiller, C., Ebert, V., Kramer, M., Peter, T., Amarouche, N., Avallone,
10   L. M., Bauer, R., Bozoki, Z., Christensen, L. E., Davis, S. M., Durry, G., Dyroff, C., Herman, R. L., Hunsmann, S., Khaykin, S. M., Mackrodt, P., Meyer, J., Smith, J. B., Spelten, N., Troy, R. F., Vomel, H., Wagner, S., and Wienhold, F. G.: The AquaVIT-1 intercomparison of atmospheric water vapor measurement techniques, Atmos Meas Tech, 7, 3177-3213, 2014.

Franc, G. D., and DeMott, P. J.: Cloud activation characteristics of airborne Erwinia carotovora cells, J Appl Meteorol, 37, 1293-1300, 1998.

15   Fröhlich-Nowoisky, J., Hill, T. C. J., Pummer, B. G., Yordanova, P., Franc, G. D., and Pöschl, U.: Ice nucleation activity in the widespread soil fungus Mortierella alpina, Biogeosciences, 12, 1057-1071, 10.5194/bg-12-1057-2015, 2015.

Govindarajan, A. G., and Lindow, S. E.: Size of bacterial ice-nucleation sites measured in situ by radiation inactivation analysis, Proceedings of the National Academy of Sciences, 85, 1334-1338, 1988.

Hader, J. D., Wright, T. P., and Petters, M. D.: Contribution of pollen to atmospheric ice nuclei concentrations, Atmos. Chem.
20   Phys., 14, 5433-5449, 10.5194/acp-14-5433-2014, 2014.

Hartmann, S., Augustin, S., Clauss, T., Wex, H., Šantl-Temkiv, T., Voigtländer, J., Niedermeier, D., and Stratmann, F.: Immersion freezing of ice nucleation active protein complexes, Atmos. Chem. Phys., 13, 5751-5766, 10.5194/acp-13-5751-2013, 2013.

Hiranuma, N., Möhler, O., Kulkarni, G., Schnaiter, M., Vogt, S., Vochezer, P., Jarvinen, E., Wagner, R., Bell, D. M., Wilson,
25   J., Zelenyuk, A., and Cziczo, D. J.: Development and characterization of an ice-selecting pumped counterflow virtual impactor (IS-PCVI) to study ice crystal residuals, Atmos Meas Tech, 9, 3817-3836, 10.5194/amt-9-3817-2016, 2016.

IPCC: Summary for Policymakers. In: Climate Change 2013: The Physical Science Basis. Contribution of Working Group I to the Fifth Assessment Report of the Intergovernmental Panel on Climate Change, Cambridge, United Kingdom and New York, NY, USA, 1–30, 2013.

Lindow, S. E., Lahue, E., Govindarajan, A. G., Panopoulos, N. J., and Gies, D.: Localization of Ice Nucleation Activity and the Icec Gene-Product in Pseudomonas-Syringae and Escherichia-Coli, Mol Plant Microbe In, 2, 262-272, Doi 10.1094/Mpmi-2-262, 1989.

Maki, L. R., and Willoughby, K. J.: Bacteria as Biogenic Sources of Freezing Nuclei, J Appl Meteorol, 17, 1049-1053, Doi 10.1175/1520-0450(1978)017<1049:Babsof>2.0.Co;2, 1978.

Möhler, O., Stetzer, O., Schaefers, S., Linke, C., Schnaiter, M., Tiede, R., Saathoff, H., Kramer, M., Mangold, A., Budz, P., Zink, P., Schreiner, J., Mauersberger, K., Haag, W., Karcher, B., and Schurath, U.: Experimental investigation of homogeneous freezing of sulphuric acid particles in the aerosol chamber AIDA, Atmos Chem Phys, 3, 211-223, 2003.

Möhler, O., DeMott, P. J., Vali, G., and Levin, Z.: Microbiology and atmospheric processes: the role of biological particles in cloud physics, Biogeosciences, 4, 1059-1071, 2007.

Möhler, O., Georgakopoulos, D. G., Morris, C. E., Benz, S., Ebert, V., Hunsmann, S., Saathoff, H., Schnaiter, M., and Wagner, R.: Heterogeneous ice nucleation activity of bacteria: new laboratory experiments at simulated cloud conditions, Biogeosciences, 5, 1425-1435, 2008.

Morris, C. E., Georgakopoulos, D. G., and Sands, D. C.: Ice nucleation active bacteria and their potential role in precipitation, J Phys Iv, 121, 87-103, DOI 10.1051/jp4:2004121004, 2004.

Murray, B. J., O'Sullivan, D., Atkinson, J. D., and Webb, M. E.: Ice nucleation by particles immersed in supercooled cloud droplets, Chem Soc Rev, 41, 6519-6554, Doi 10.1039/C2cs35200a, 2012.

O'Sullivan, D., Murray, B. J., Ross, J. F., and Webb, M. E.: The adsorption of fungal ice-nucleating proteins on mineral dusts: a terrestrial reservoir of atmospheric ice-nucleating particles, Atmos. Chem. Phys., 16, 7879-7887, 10.5194/acp-16-7879-2016, 2016.

Oehm, C. C., C.; Amato, P.; Attard, E.; Delort, A.-M.; Morris, C.; Kiselev, A.; Stetzer, O.; Möhler, O.; Leisner, T.: Laboratory studies with cloud-derived Bacterial Cells acting as Ice Nuclei in the Immersion and Deposition Mode, EGU General Assembly 2012, Vienna, Austria, 2012, 399,

Pratt, K. A., DeMott, P. J., French, J. R., Wang, Z., Westphal, D. L., Heymsfield, A. J., Twohy, C. H., Prenni, A. J., and Prather, K. A.: In situ detection of biological particles in cloud ice-crystals, Nature Geosci, 2, 398-401 (SI section), http://www.nature.com/ngeo/journal/v2/n6/suppinfo/ngeo521_S1.html, 2009.

Pruppacher, H. R., and Klett, J. D.: Microphysics of Clouds and Precipitation, Atmospheric and Oceanographic Sciences Library, Springer Netherlands, 2010.

Pummer, B. G., Bauer, H., Bernardi, J., Bleicher, S., and Grothe, H.: Suspendable macromolecules are responsible for ice nucleation activity of birch and conifer pollen, Atmos. Chem. Phys., 12, 2541-2550, 10.5194/acp-12-2541-2012, 2012.

Šantl-Temkiv, T., Sahyoun, M., Finster, K., Hartmann, S., Augustin-Bauditz, S., Stratmann, F., Wex, H., Clauss, T., Nielsen, N. W., Sørensen, J. H., Korsholm, U. S., Wick, L. Y., and Karlson, U. G.: Characterization of airborne ice-nucleation-active bacteria and bacterial fragments, Atmospheric Environment, 109, 105-117, http://dx.doi.org/10.1016/j.atmosenv.2015.02.060, 2015.

5   Schnell, R. C., and Vali, G.: Biogenic Ice Nuclei: Part I. Terrestrial and Marine Sources, Journal of the Atmospheric Sciences, 33, 1554-1564, 10.1175/1520-0469(1976)033<1554:BINPIT>2.0.CO;2, 1976.

Sharma, P. K., and Rao, K. H.: Analysis of different approaches for evaluation of surface energy of microbial cells by contact angle goniometry, Adv Colloid Interfac, 98, 341-463, Pii S0001-8686(02)00004-0

Doi 10.1016/S0001-8686(02)00004-0, 2002.

10  Simpson, E. L., Connolly, P. J., and McFiggans, G. B.: Competition for water vapour results in suppression of ice formation in mixed phase clouds, Atmos. Chem. Phys. Discuss., 10.5194/acp-2017-673, 2017.

Vaden, T. D., Imre, D., Beranek, J., and Zelenyuk, A.: Extending the Capabilities of Single Particle Mass Spectrometry: I. Measurements of Aerosol Number Concentration, Size Distribution, and Asphericity, Aerosol Sci Tech, 45, 113-124, Doi 10.1080/02786826.2010.526155, 2011a.

15  Vaden, T. D., Imre, D., Beranek, J., and Zelenyuk, A.: Extending the Capabilities of Single Particle Mass Spectrometry: II. Measurements of Aerosol Particle Density without DMA, Aerosol Sci Tech, 45, 125-135, Doi 10.1080/02786826.2010.526156, 2011b.

Vali, G., DeMott, P. J., Möhler, O., and Whale, T. F.: Technical Note: A proposal for ice nucleation terminology, Atmos Chem Phys, 15, 10263-10270, 2015.

20  Wagner, R., and Möhler, O.: Heterogeneous ice nucleation ability of crystalline sodium chloride dihydrate particles, J Geophys Res-Atmos, 118, 4610-4622, 2013.

Wex, H., Augustin-Bauditz, S., Boose, Y., Budke, C., Curtius, J., Diehl, K., Dreyer, A., Frank, F., Hartmann, S., Hiranuma, N., Jantsch, E., Kanji, Z. A., Kiselev, A., Koop, T., Möhler, O., Niedermeier, D., Nillius, B., Rosch, M., Rose, D., Schmidt, C., Steinke, I., and Stratmann, F.: Intercomparing different devices for the investigation of ice nucleating particles using
25  Snomax (R) as test substance, Atmos Chem Phys, 15, 1463-1485, 10.5194/acp-15-1463-2015, 2015.

Wolber, P. K., Deininger, C. A., Southworth, M. W., Vandekerckhove, J., Vanmontagu, M., and Warren, G. J.: Identification and Purification of a Bacterial Ice-Nucleation Protein, P Natl Acad Sci USA, 83, 7256-7260, DOI 10.1073/pnas.83.19.7256, 1986.

Wolf, R., Slowik, J. G., Schaupp, C., Amato, P., Saathoff, H., Möhler, O., Prevot, A. S. H., and Baltensperger, U.: Characterization of ice-nucleating bacteria using on-line electron impact ionization aerosol mass spectrometry, J Mass Spectrom, 50, 662-671, 10.1002/jms.3573, 2015.

Yankofsky, S. A., Levin, Z., Bertold, T., and Sandlerman, N.: Some Basic Characteristics of Bacterial Freezing Nuclei, J Appl Meteorol, 20, 1013-1019, Doi 10.1175/1520-0450(1981)020<1013:Sbcobf>2.0.Co;2, 1981.

Zawadowicz, M. A., Froyd, K. D., Murphy, D. M., and Cziczo, D. J.: Improved identification of primary biological aerosol particles using single-particle mass spectrometry, Atmos. Chem. Phys., 17, 7193-7212, 10.5194/acp-17-7193-2017, 2017.

Zelenyuk, A., Cuadra-Rodriguez, L. A., Imre, D., Shimpi, S., and Warey, A.: Comprehensive Characterization Of Ultrafine Particulate Emission From 2007 Diesel Engines: PM Size Distribution, Loading And Individual Particle Size And Composition, *Eos Trans. AGU*, 2006, Abstract A43A-0121,

Zelenyuk, A., Imre, D., Nam, E. J., Han, Y. P., and Mueller, K.: ClusterSculptor: Software for expert-steered classification of single particle mass spectra, International Journal of Mass Spectrometry, 275, 1-10, DOI 10.1016/j.ijms.2008.04.033, 2008.

Zelenyuk, A., Imre, D., Wilson, J., Zhang, Z. Y., Wang, J., and Mueller, K.: Airborne Single Particle Mass Spectrometers (SPLAT II & miniSPLAT) and New Software for Data Visualization and Analysis in a Geo-Spatial Context, J Am Soc Mass Spectr, 26, 257-270, 10.1007/s13361-014-1043-4, 2015.
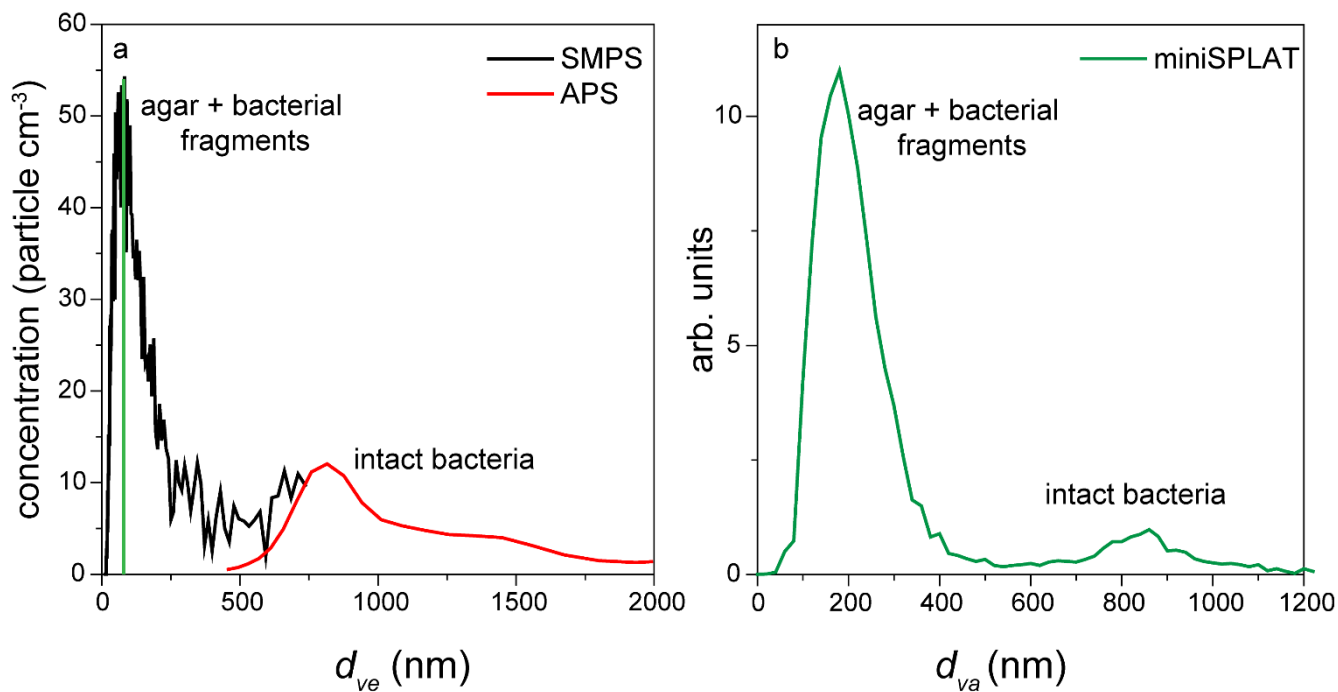
**Figure 1: Size distributions of an aerosolized suspension of Pseudomonas syringae in the AIDA cloud chamber before Expansion 1, calculated based on the SMPS and the APS measurements (a) and miniSPLAT (b). The miniSPLAT small particle detection limit is denoted by the green line in (a).**
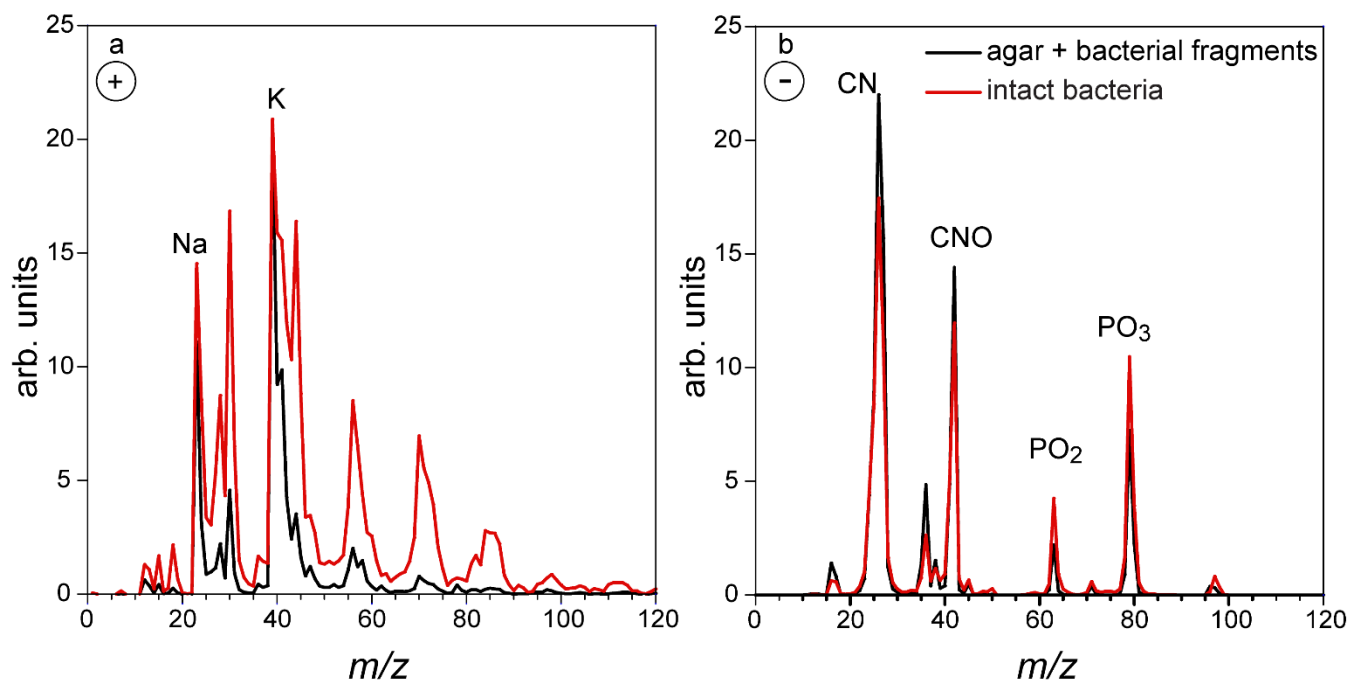
**Figure 2: Positive (a) and negative (b) mass spectra of the particles in the AIDA chamber, measured before Expansion 1. Reference mass spectra of the small size mode, made up of agar mixed with bacterial fragments, which includes particles smaller than 300 nm, are marked in black, and the mass spectra of the large size mode particles ($d_{va}$ > 700 nm), composed of intact Pseudomonas syringae bacterial cells, are marked in red.**
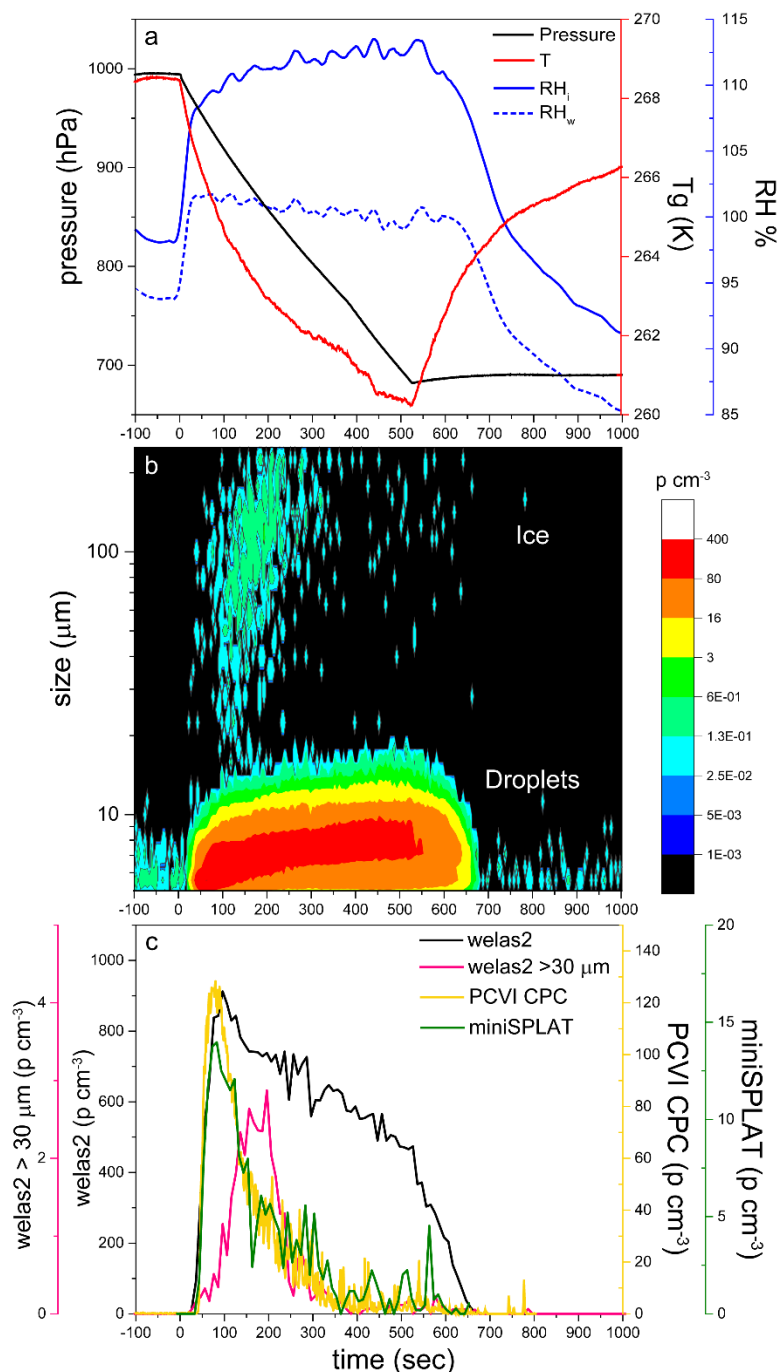
**Figure 3: Data from Expansion 1. (a) The pressure (black) and the temperature of the gas (red) inside the AIDA chamber. The measured RH with respect to ice (RHi) and water (RHw) are indicated in solid and dashed blue lines, respectively; (b) the size distributions of the particles measured with welas2 during the expansion. Particles smaller than ~15 µm are liquid droplets, while particles with larger optical diameters are ice; (c) The welas2-measured total particle number concentrations (black) and the number concentrations of particles larger than 30 µm (pink). The number concentrations of particles transmitted by the PCVI and measured by CPC and miniSPLAT are marked in yellow and green, respectively.**
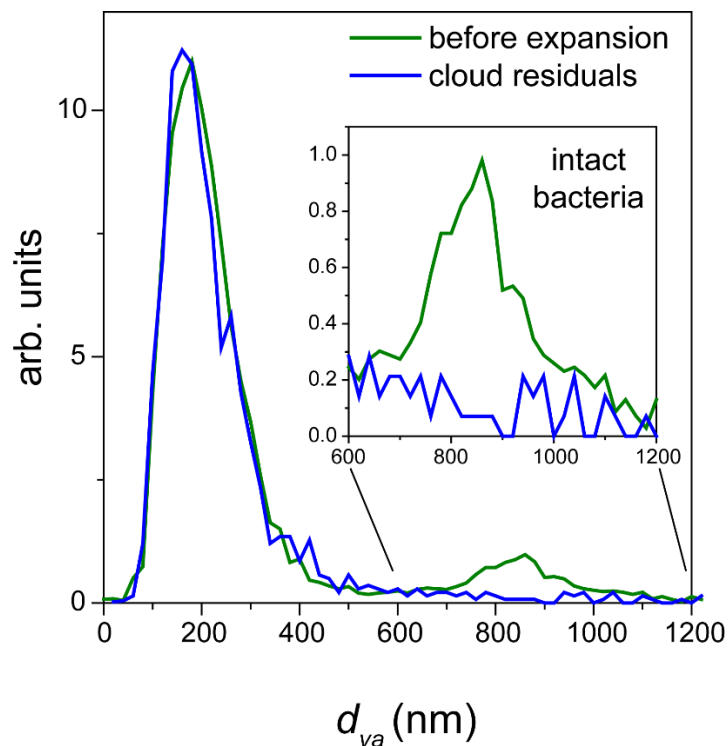
**Figure 4: Normalized miniSPLAT-measured $d_{va}$ size distributions of particles in the AIDA chamber before Expansion 1 (green) and of cloud residuals transmitted through the PCVI during the expansion (blue). The inset presents in expanded scale the size distributions of the intact bacteria, showing that cloud residuals do not exhibit the distinct peak for intact bacteria.**
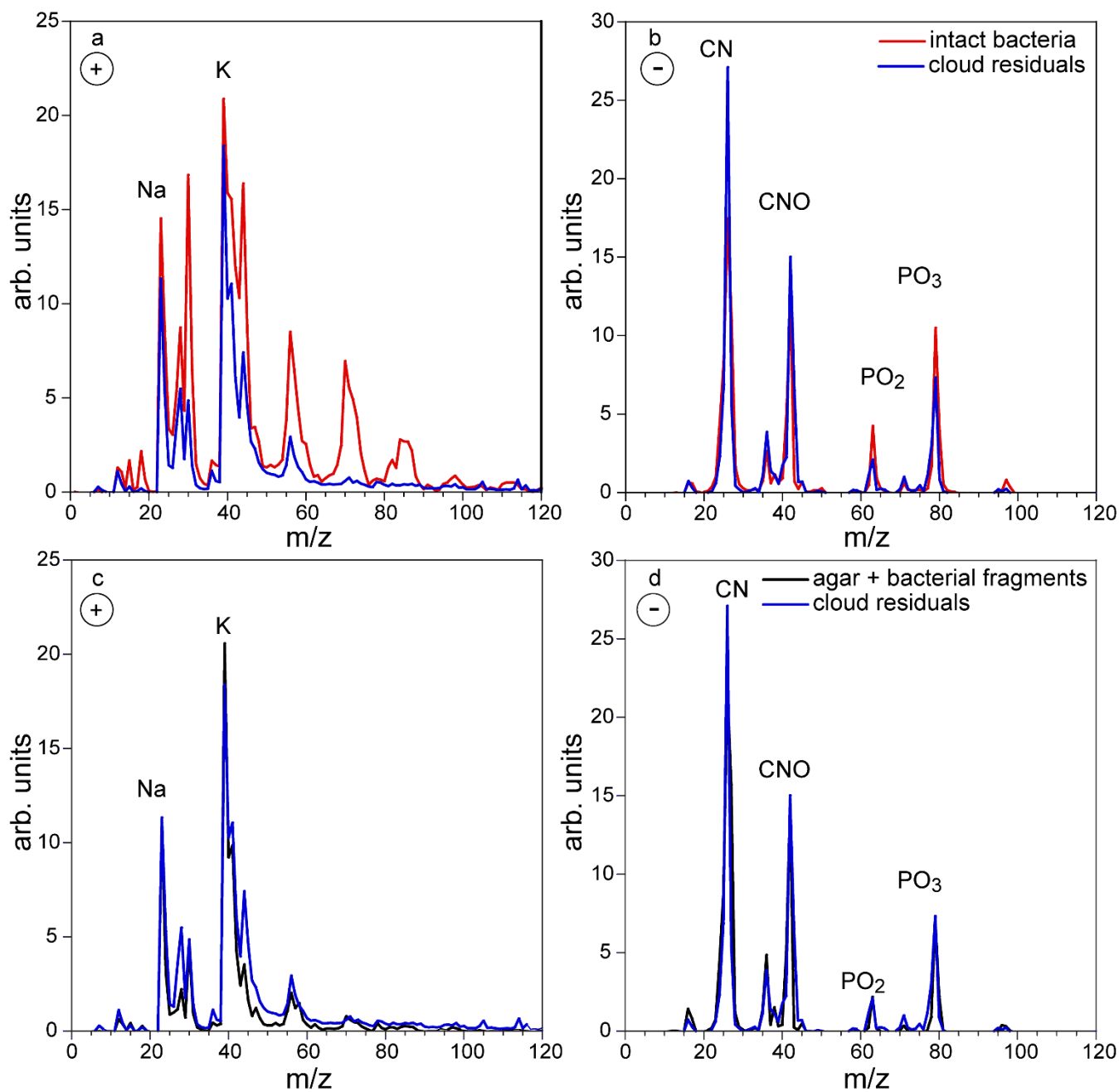
**Figure 5: Positive (a) and negative (b) ion mass spectra of cloud residuals sampled during Expansion 1 (blue) superimposed on the MS of intact bacteria (red); (c) and (d) The same cloud residuals MS superimposed on the reference MS of the small particle mode, composed of bacterial fragments mixed with agar (black).**
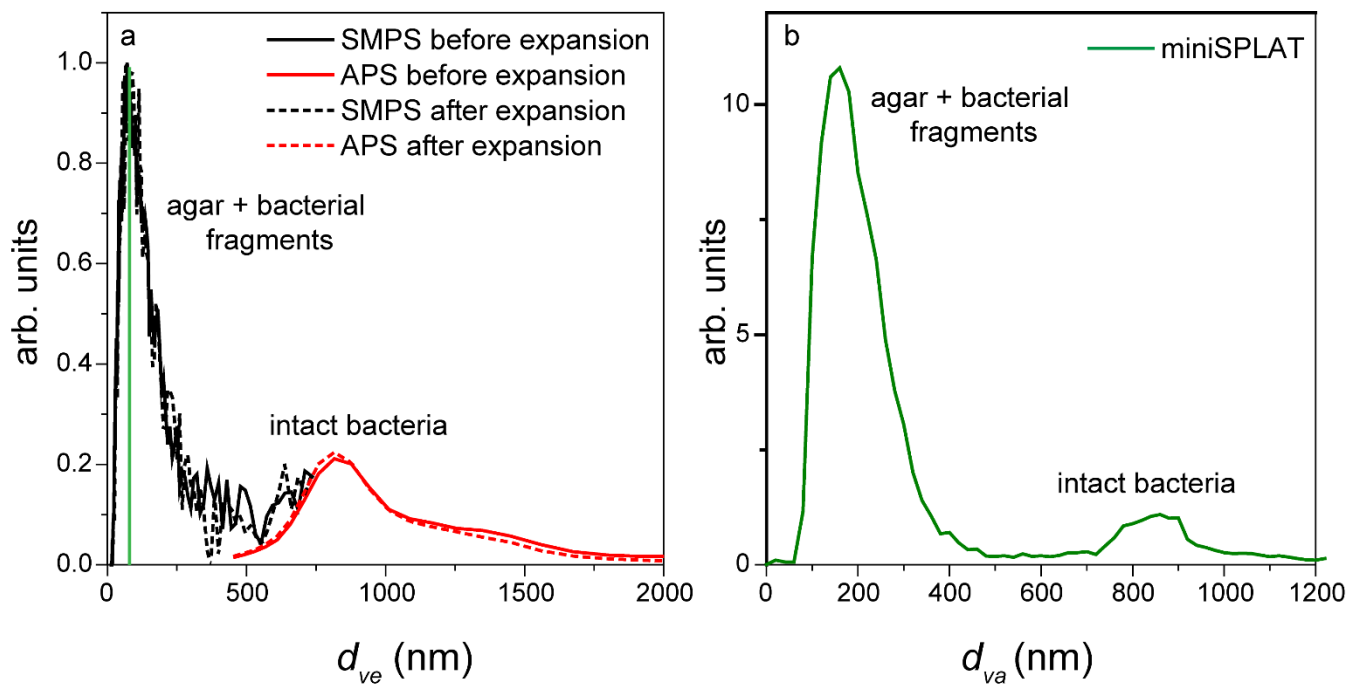
**Figure 6: (a) Size distributions of an aerosolized suspension of PF CGina particles in the AIDA cloud chamber before and after Expansion 2 calculated from the SMPS and the APS measurements; (b) miniSPLAT-measured size distribution of PF CGina particles in the chamber before Expansion 2. The miniSPLAT small particle detection limit is denoted by the green line in (a).**
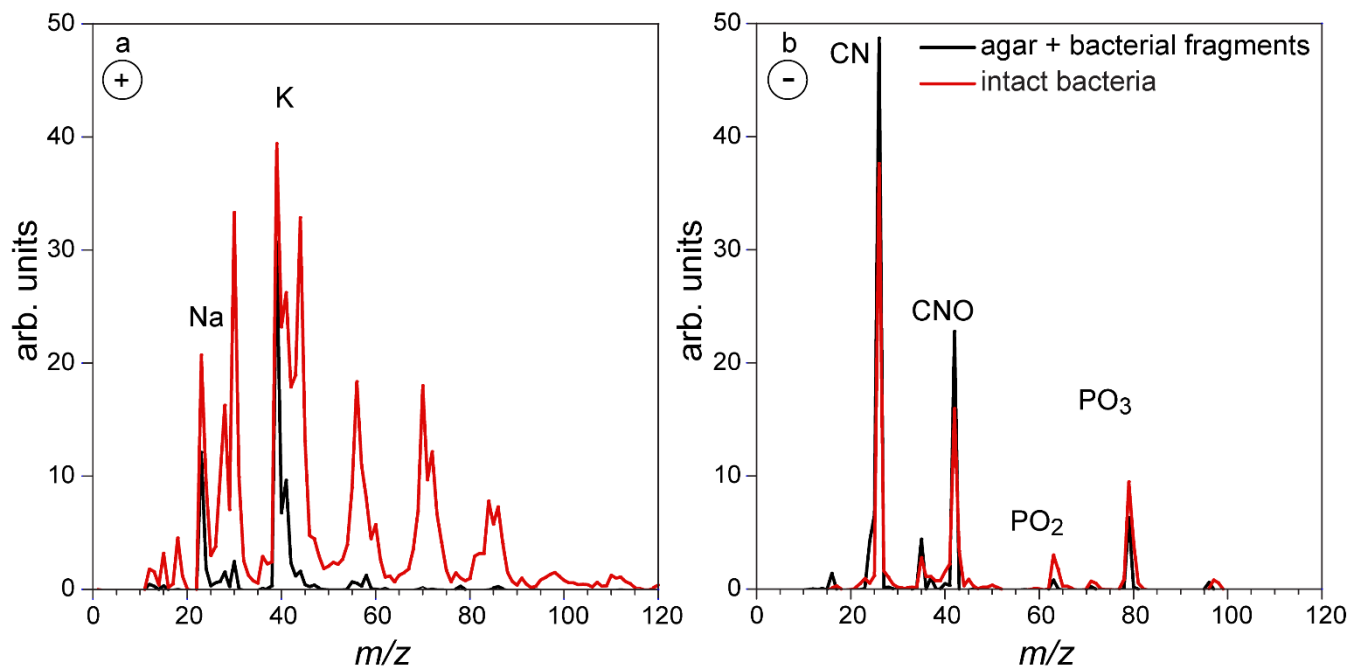
Figure 7: Positive (a) and negative (b) mass spectra of the particles in the AIDA chamber, measured before Expansion 2. Reference mass spectra of the small size mode, made up of particles smaller than 300 nm (black), and the mass spectra of the large size mode (>700 nm) composed of intact PF CGina bacterial cells are marked in red.
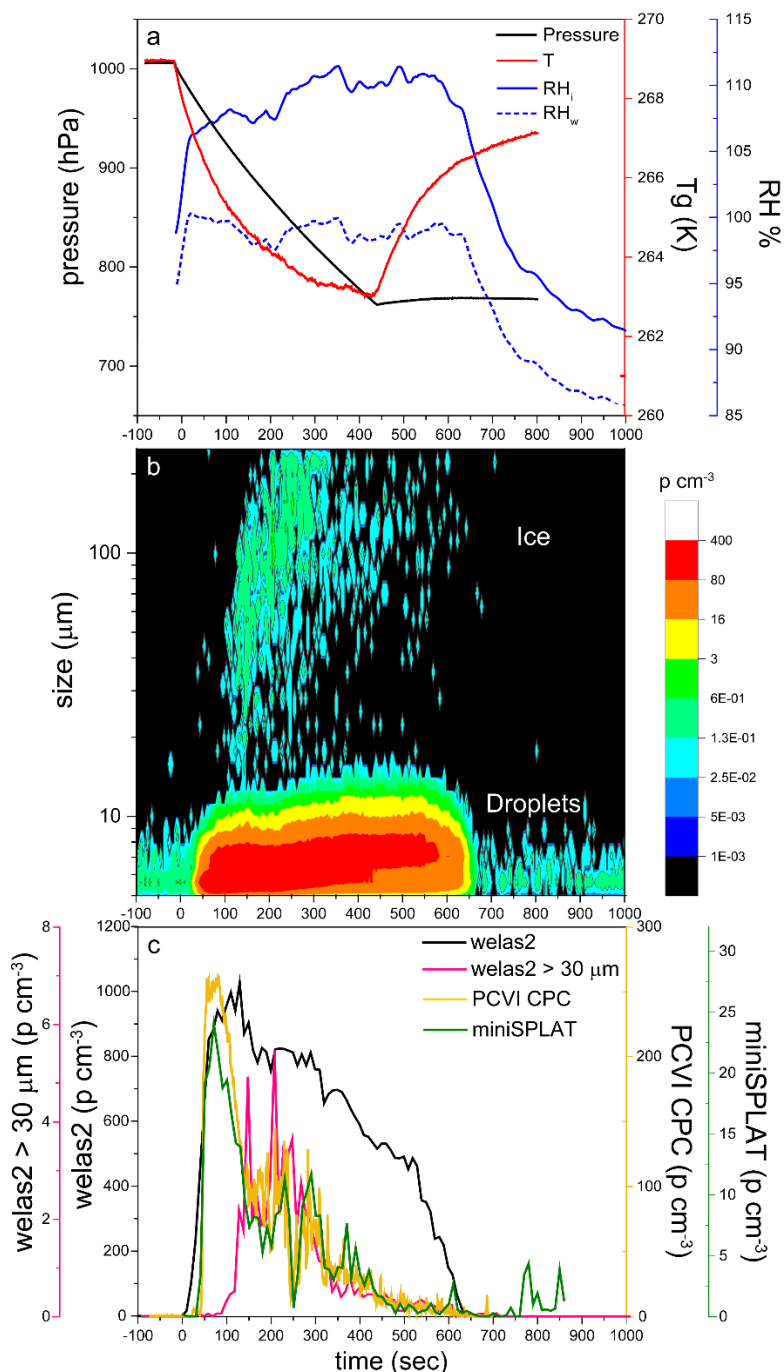
**Figure 8: Data from Expansion 2. (a) The pressure (black) and the temperature of the gas (red) inside the AIDA chamber. The measured RH with respect to ice (RHi) and water (RHw) are indicated in solid and dashed blue lines, respectively; (b) the size distributions of the particles measured with welas2 during the expansion. Particles smaller than ~15 μm are liquid droplets, while larger particles are ice; (c) The welas2-measured total particle number concentrations (black) and the number concentrations of particles larger than 30 μm (pink). The number concentrations of particles transmitted by the PCVI and measured by CPC and miniSPLAT are marked in yellow and green, respectively.**
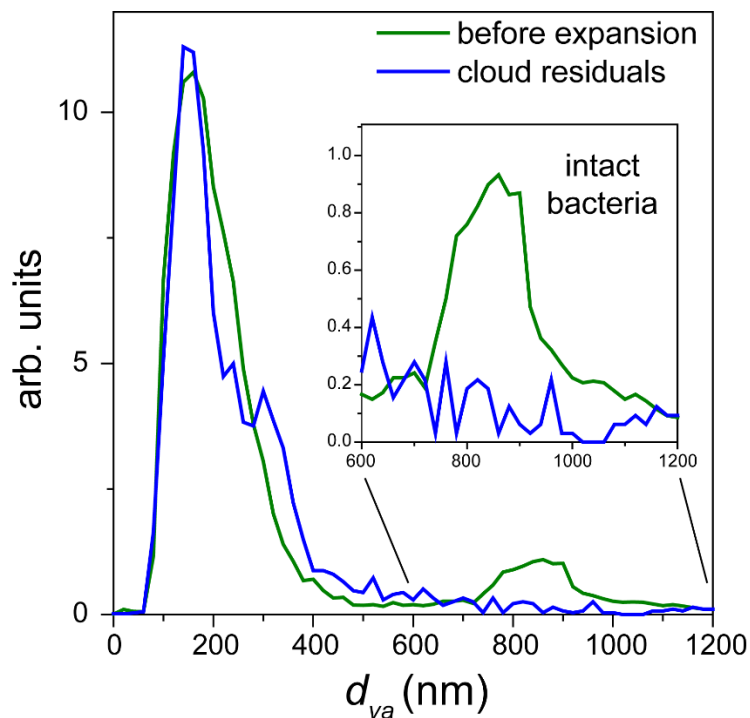
**Figure 9: Normalized miniSPLAT-measured $d_{va}$ size distributions of particles in the AIDA chamber before Expansion 2 (green) and of cloud residuals transmitted through the PCVI during the expansion (blue). The inset presents in expanded scale the size distributions of the intact bacteria, showing that nearly no distinct peak for intact bacteria.**
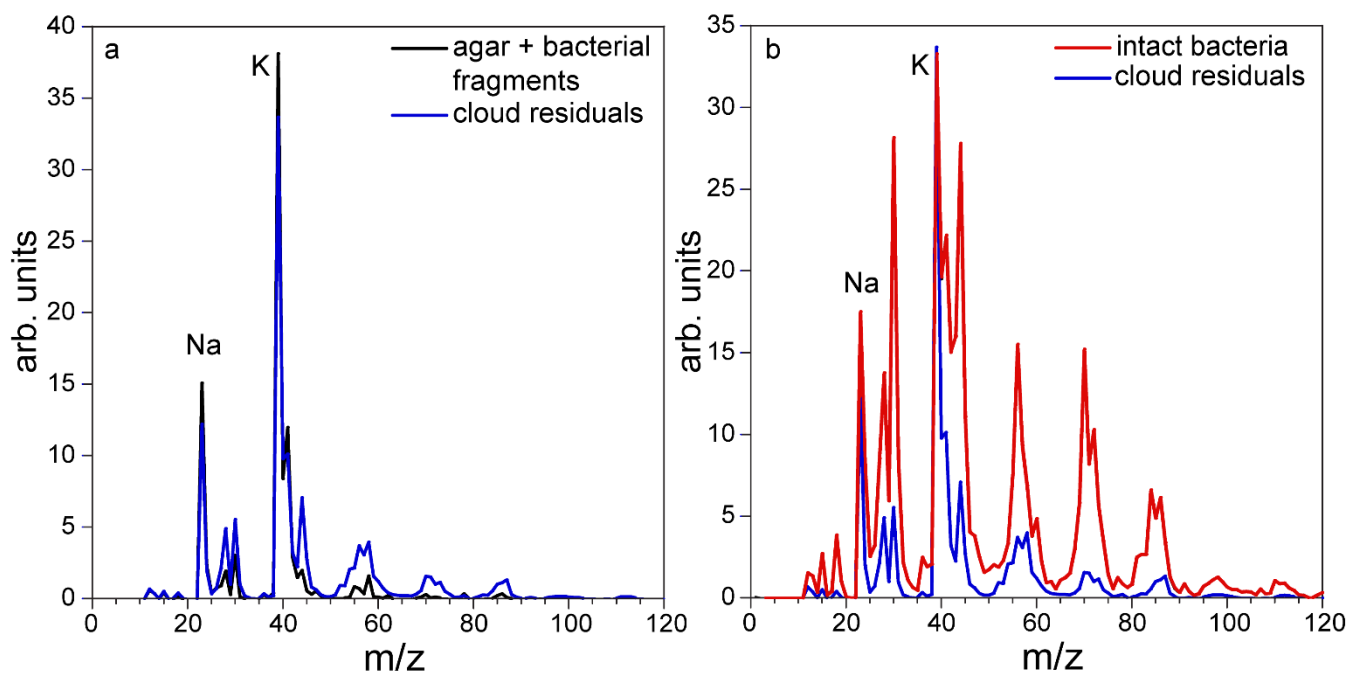
Figure 10: (a) Reference MS of the small particle mode, composed of agar and bacterial fragments, (black) and the MS of cloud residuals acquired during Expansion 2 (blue); (b) MS of intact bacteria (red) and the MS of cloud residuals acquired during
5    Expansion 2 (blue).
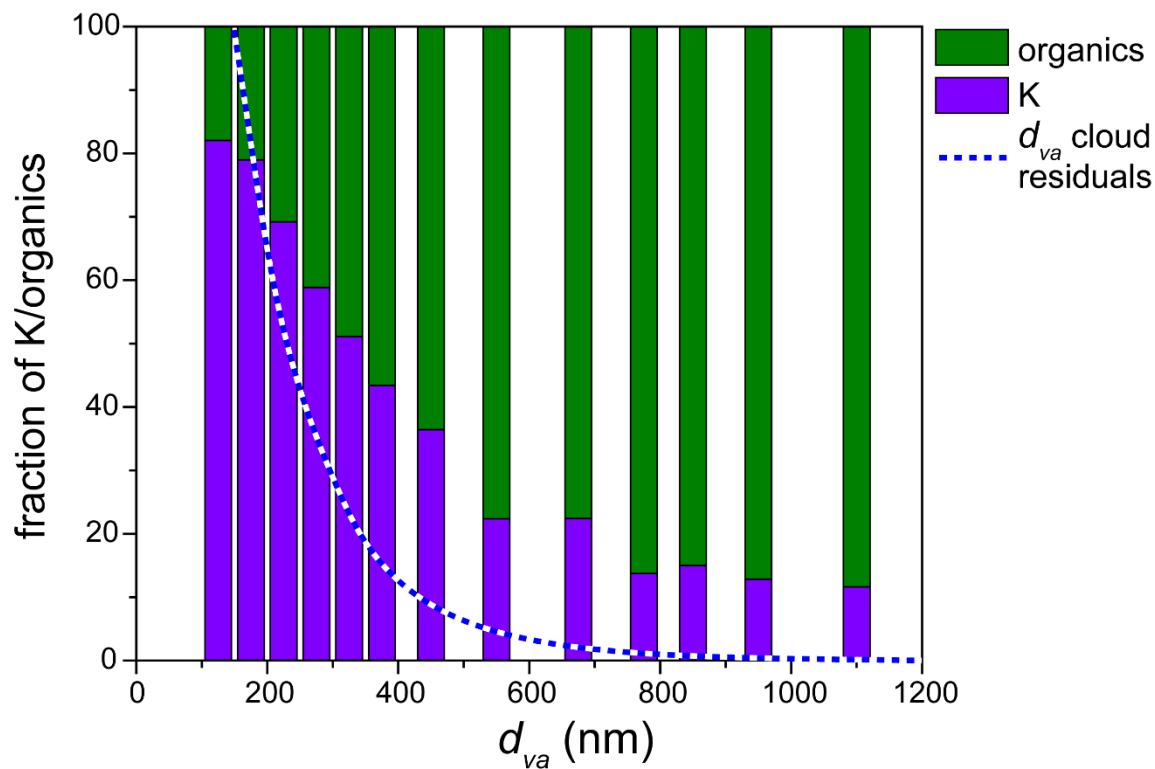
**Figure 11: The relative mass spectral intensity of peaks assigned to organics and potassium as a function of particle $d_{va}$, showing that larger particles contain more organics. The dashed line represents the measured $d_{va}$ distribution of cloud residuals.**
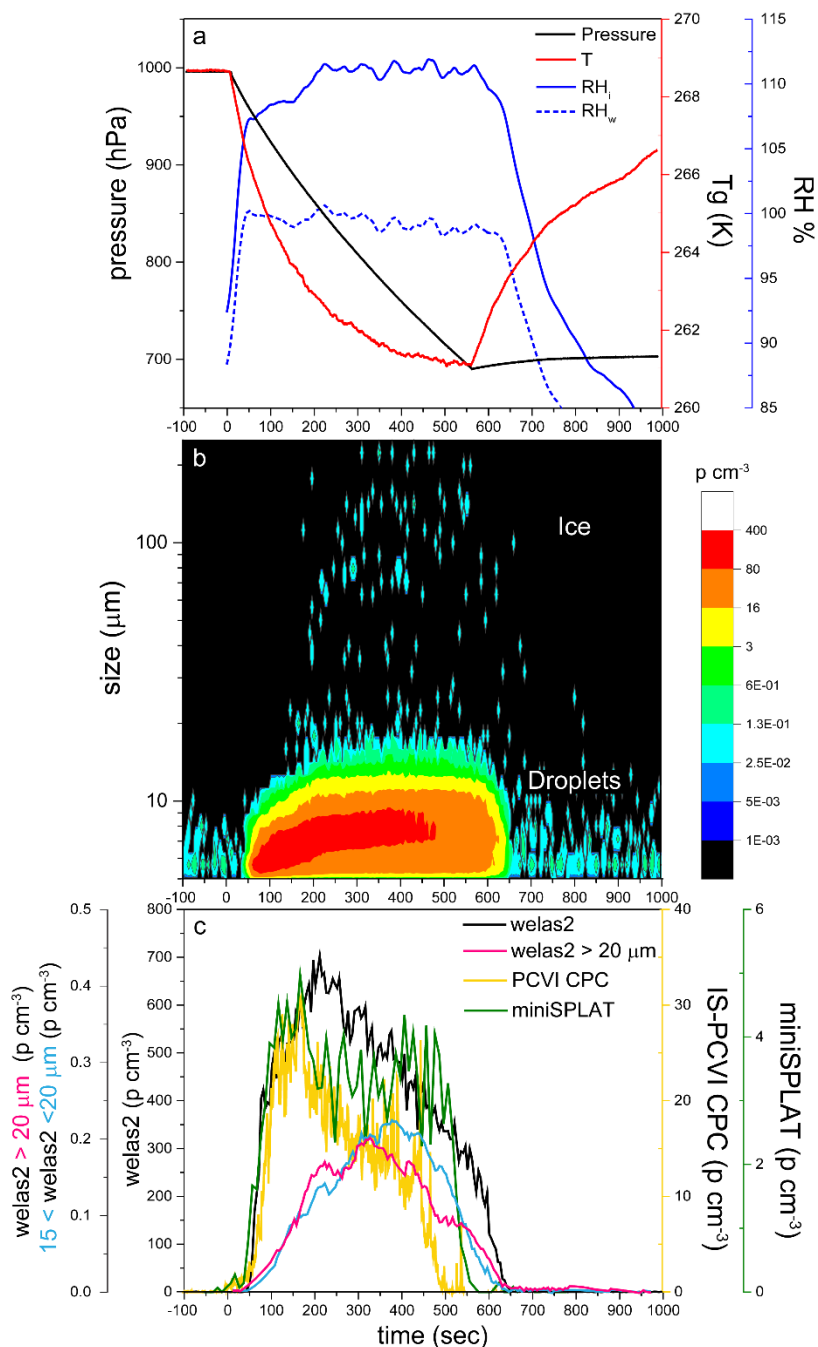
**Figure 12: Data from Expansion 3. (a) The pressure (black) and the temperature of the gas (red) inside the AIDA chamber. The measured RH with respect to ice (RHi) and water (RHw) are indicated in solid and dashed blue lines, respectively; (b) the size distributions of the particles measured with welas2 during the expansion. Particles smaller than ~15 μm are liquid droplets, while larger particles are ice; (c) The welas2-measured total particle number concentrations (black), the number concentrations of particles larger than 15 μm, but smaller than 20 μm (light blue), and the number concentrations of particles larger than 20 μm (pink). The CPC and miniSPLAT measured number concentrations of particles transmitted by the PCVI are marked in yellow and green, respectively.**
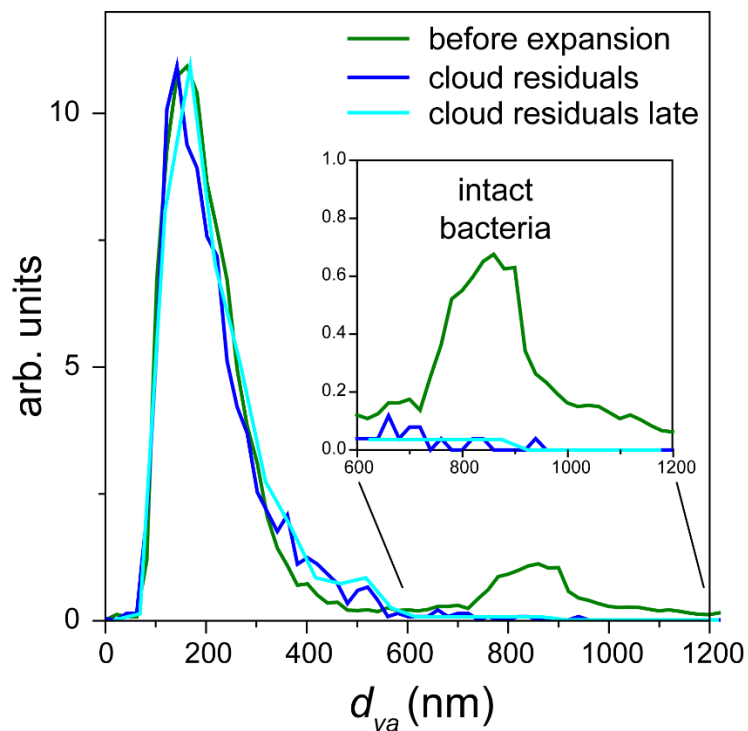
**Figure 13:** $d_{va}$ **size distribution measured by miniSPLAT before Expansion 3 (green), of cloud residuals (blue), and of cloud residuals measured during the later part of the expansion when the number concentration of sampled droplets and ice crystals were nearly the same (light blue). The inset shows an expanded scale of the region of intact bacteria.**
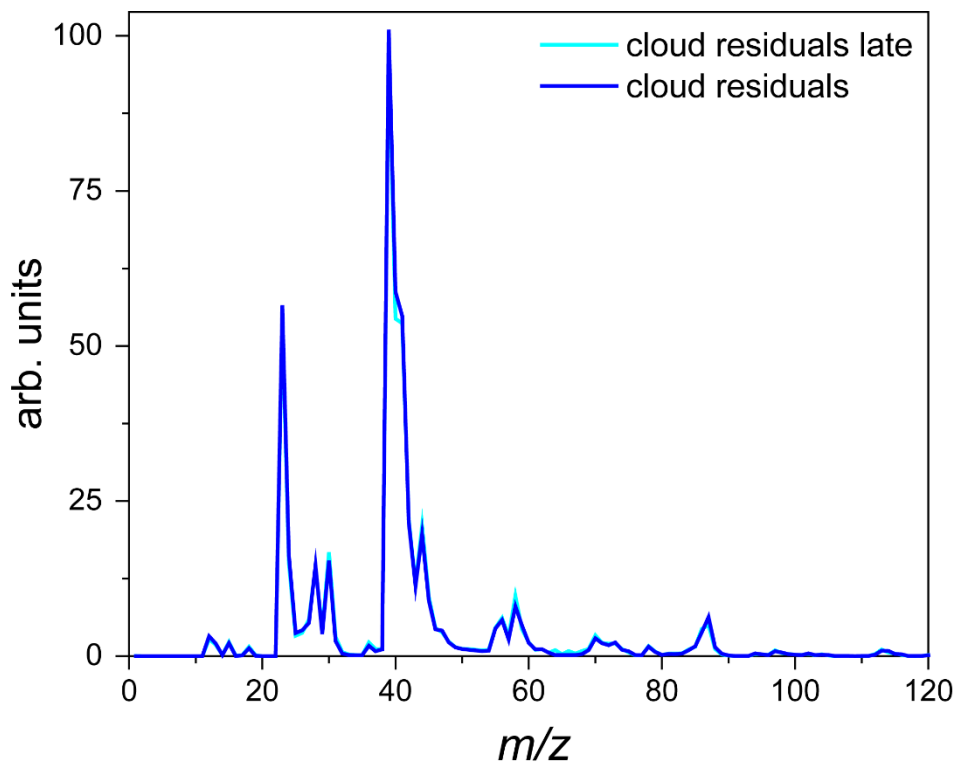
**Figure 14: Average mass spectrum of cloud residuals measured during Expansion 3 (blue) super imposed on the mass spectrum of particles characterized later in the expansion when the number of sampled ice crystals and cloud droplets were comparable (light blue).**